Ion Channels

International Edition: DOI: 10.1002/anie.201916287
German Edition: DOI: 10.1002/ange.201916287

Polyhydrazide-Based Organic Nanotubes as Efficient and Selective Artificial Iodide Channels

Arundhati Roy[+], Himanshu Joshi[+], Ruijuan Ye, Jie Shen, Feng Chen, Aleksei Aksimentiev, and Huaqiang Zeng**

Abstract: *Reported herein is a series of pore-containing polymeric nanotubes based on a hydrogen-bonded hydrazide backbone. Nanotubes of suitable lengths, possessing a hollow cavity of about a 6.5 Å diameter, mediate highly efficient transport of diverse types of anions, rather than cations, across lipid membranes. The reported polymer channel, having an average molecular weight of 18.2 kDa and 3.6 nm in helical height, exhibits the highest anion-transport activities for iodide (EC_{50} = 0.042 μM or 0.028 mol% relative to lipid), whcih is transported 10 times more efficiently than chlorides (EC_{50} = 0.47 μM). Notably, even in cholesterol-rich environment, iodide transport activity remains high with an EC_{50} of 0.37 μM. Molecular dynamics simulation studies confirm that the channel is highly selective for anions and that such anion selectivity arises from a positive electrostatic potential of the central lumen rendered by the interior-pointing methyl groups.*

Introduction

Transport of anions is crucial for precise regulation of physiological processes.[1] As one of the essential elements of our body, iodides help to synthesize thyroid hormones, that is, triiodothyronine and thyroxine.[2] They also help in proper bone development, that is, skeletal growth. The Na^+/I^- symporter (NIS) is a transmembrane glycoprotein that was identified to facilitate I^- transport into the follicular cells of thyroid gland, a first step in thyroid hormone biosynthesis.[3] Since most of the thyroid and breast cancers expresses NIS, radioactive ^{131}I has been routinely used for the imaging and treatment of these cancers. However, most of the times, they express insufficient NIS and thus triggers feeble uptake of ^{131}I. Further, dysregulation of I^- through NIS causes iodide deficiency disorders (IDDs)[4] on key organs such as the brain, kidney, liver, heart, and muscle.

Considerable interest has been invested in developing ion-transport machinery for selective transport of chloride in lipid bilayer membranes.[5] This endeavor is not only to understand the fundamental transport mechanism in biology but also for possible medical applications in either channelopathies[6] or as anticancer agents.[5m,7] However, synthetic iodide channels are still underexplored, considering that only two iodide-selective channels have been reported thus far.[8] The first iodide channel was reported by the group of Gin and is based on a β-cyclodextrin, exhibiting low activity and low selectivity among halides ($I^- > Br^- > Cl^-$).[8a] Recent work by the group of Kim has shown that a porphyrin-based covalent organic cage can achieve high I^-/Cl^- selectivity but with quite moderate iodide transport activity.[8b] As such, there is a need to develop highly active and selective artificial iodide transporters for potential medical treatment of IDD.

In 2004, the group of Li reported a series of hydrazide-based aromatic foldamers that can fold by intramolecular hydrogen-bonds into well-defined cavity-containing curved conformations (for its general structure, see Figure 1), with the longest heptamer taking a one-turn helical structure.[9] Later on, the same group prepared short oligomers containing 5 to 11 building blocks, as well as a short polymer sample having 20 building blocks and a helical height of 1.1 nm.[10] Exterior modification using triphenylalanine-based side-chains enables these molecules to transport cations over anions on order of $NH_4^+ > Cs^+ > Rb^+ > K^+ > Na^+$.

Nevertheless, a large dimension of 9 Å × 11 Å (W × H; see Figure S1 in the Supporting Information) of the triphenylalanine side-chains, which is not compatible with a typical aromatic π–π stacking distance of 3.4 Å, might distort the central helical backbone and alter its intrinsic ion transport properties. This perspective prompted us to prepare longer polymers, containing only straight alkyl chains arrayed around the exterior, to examine the true ion-transporting properties.

Our motivation to prepare longer polymers is geared toward producing fully hydrogen-bonded, helically folded, cavity-containing nanotubes that can span the hydrophobic region of a lipid membrane (ca. 3.4 nm, Figure 1). Achieving this goal through polymerization has proven to be a challenging task,[11] and can mostly be ascribed to the low reactivity of amines and carboxylic acids, which are destined to form covalent bonds but are highly rigidified by intramolecular hydrogen bonds. In fact, despite availability of diverse types of fully hydrogen-bonded aromatic foldamers[12] reported

[*] Dr. A. Roy,[+] Dr. J. Shen, Dr. F. Chen, Dr. H. Zeng
NanoBio Lab
31 Biopolis Way, The Nanos, Singapore 138669 (Singapore)
E-mail: hqzeng@nbl.a-star.edu.sg
Dr. H. Joshi,[+] Prof. Dr. A. Aksimentiev
Department of Physics and Beckman Institute for Advanced Science and Technology, University of Illinois at Urbana-Champaign
Urbana, IL 61801 (USA)
E-mail: aksiment@illinois.edu
R. Ye
Department of Chemical and Biomolecular Engineering, National University of Singapore, Singapore 117585 (Singapore)
[+] These authors contributed equally to this work.
Supporting information and the ORCID identification number(s) for the author(s) of this article can be found under: https://doi.org/10.1002/anie.201916287.

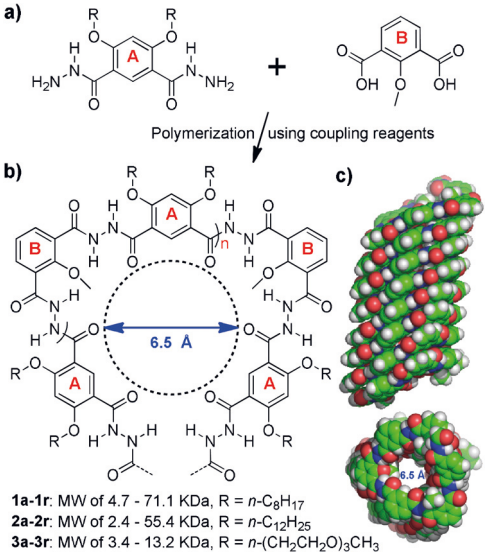

Figure 1. a) Structures of building blocks **A** and **B** used to produce nanotubes **1**–**3**. b) Foldamer-based approach for constructing hydrogen-bonded pore-forming polymeric anion channels **1**–**3**, having a hollow cavity of 6.5 Å in diameter after excluding van der Waals volume of atoms decorating the channel's interior. c) Side and top views of a helically folded polymeric nanotube computationally optimized in the POPC membrane (see the Supporting Information).

since the pioneering reports,[13] the hitherto reported longest nanotube with a fully hydrogen-bonded aromatic tubular cavity carries an average of 30 repeating units and a helical height of 1.4 nm,[11a,14] while partially hydrogen-bonded polymers with a more flexible backbone could reach 6.1 nm.[11a]

In this work, we, for the first time, report successful production of fully hydrogen-bonded, helically folded polymeric foldamers that possess a long tubular cavity with as much as 14 nm in height, by polymerization of two readily accessible repeating units, **A** and **B** (Figure 1). Importantly, our above surmise turns out to work out perfectly well, although in a somewhat surprising fashion. That is, in sharp contrast to preferred transport of cations over anions as reported by Li,[10] we demonstrate that alkyl-chain-appended polymers of 2.1–5.4 nm with a helical height and about a 6.5 Å cavity diameter (Figure 1c), promote a highly selective transport of anions, rather than cations, across lipid membranes.

Results and Discussion

Synthesis of long polymers of 2.1–5.4 nm in helical height

Early attempts to prepare fully hydrogen-bonded polymeric aromatic foldamers often used the acyl chloride coupling method.[10,11a] Following this method to test a few polymerization conditions for coupling **A** and **B**, we found that 6.7 kDa (about 3.9 helical turns and 1.3 nm in helical height) is about the highest molecular weight we can obtain (entry 18 of Table S1 in the Supporting Information). This is consistent with 1.1 nm in height obtained by Li for the same type of polymers with different side chains.[10]

Encouraged by our recent findings that the amide coupling reagent BOP could mediate efficient formation of sterically hindered hydrogen-bond-rigidified amide bonds,[15] we decided to scrutinize the polymerization efficacy of 17 amide coupling agents. For convenience of recording, polymers with exterior side-chains are classified as **1** (R = *n*-C_8H_{17}), **2** (R = *n*-$C_{12}H_{25}$), and **3** (R = *n*-$(CH_2CH_2O)_3CH_3$), while the letters **a**–**r** designate one of the 18 coupling methods (17 coupling agents + acyl chloride) used to produce the polymer samples (Figure 2b; see Table S1). For instance, the polymer **1a** refers to a polymer sample with *n*-C_8H_{17} as side-chains and HATU as the coupling agent.

The units **A** containing three types of side chains were made from resorcinol by following a three-step protocol, and subsequent reaction with hydrazine hydrate.[16] The optimized polymerization conditions involve mixing **A**, **B**, and the coupling agent at a molar ratio of 1:1:3 in 6 mL of freshly distilled CH_2Cl_2/DMF (5:1, v:v) at room temperature, followed by addition of 100 μL DIEA (*N*,*N*-diisopropylethylamine). The polymerization reaction proceeded for 2 days, with typical yields of 60–80% for a total of 53 polymer samples (e.g., **1a**–**r** except for **1h**, **2a**–**r**, and **3a**–**r**). Their average molecular weights were determined by gel-permeation chromatography and are listed in Table S1. Polymers **1a**, **1c**, **2a**, **2c**, and **3c** displayed characteristic mass patterns of a repeating unit in the MALDI spectra (see Figures S2–S6).

Efficient ion transport by polymer channels

We evaluated the ability of these polymers to plug into a lipid membrane and to transport ions across the membrane using a fluorescence assay (Figure 2a), which employs the pH-sensitive fluorescent dye HPTS (8-hydroxy-1,3,6-pyrenetrisulfonate) trapped inside egg yolk phosphatidylcholine (EYPC) based, large unilamellar vesicles (LUVs).[5a,17] In this assay, a pH gradient of 7 to 8 was applied across the vesicles, and ion-transport activities were monitored by the incremental changes in the HPTS fluorescence (λ_{ex} = 450 nm, λ_{em} = 510 nm) over a 300 second period with that induced by Triton X-100 (added at t = 300 s) set as 100% (Figure 2b).

Application of this pH-sensitive HPTS assay onto 17 polymer samples with *n*-C_8H_{17} side chains (**1a**–**g** and **1i**–**r**, Figure 2b) reveals that **1a**, having an average molecular weight of 18.2 KDa and a height of 3.6 nm,[5c] exhibits the highest fractional transport activity of 102% at 1 μM. This high activity was followed by **1k** (100%), **1m** (97%), **1d** (77%), **1c** (73%), and **1b** (68%), with molecular weights of 10.8–27.3 kDa and heights of 2.1–5.4 nm. The remaining 11 samples, with low fractional activities of less than 25%, are characterized by low (< 10 kDa) or high (> 30 kDa) molecular weights. These results are largely consistent with hydrophobic membrane thickness of 3.4 nm.

As summarized in Figures 2c, and Figures S12 and S13, using the same HPTS assay at the same concentration (1 μM), the best channels for series **2** and **3** are **2h** (15%, MW = 33 KDa) and **3d** (37%, MW = 3.4 kDa), respectively. Generally,

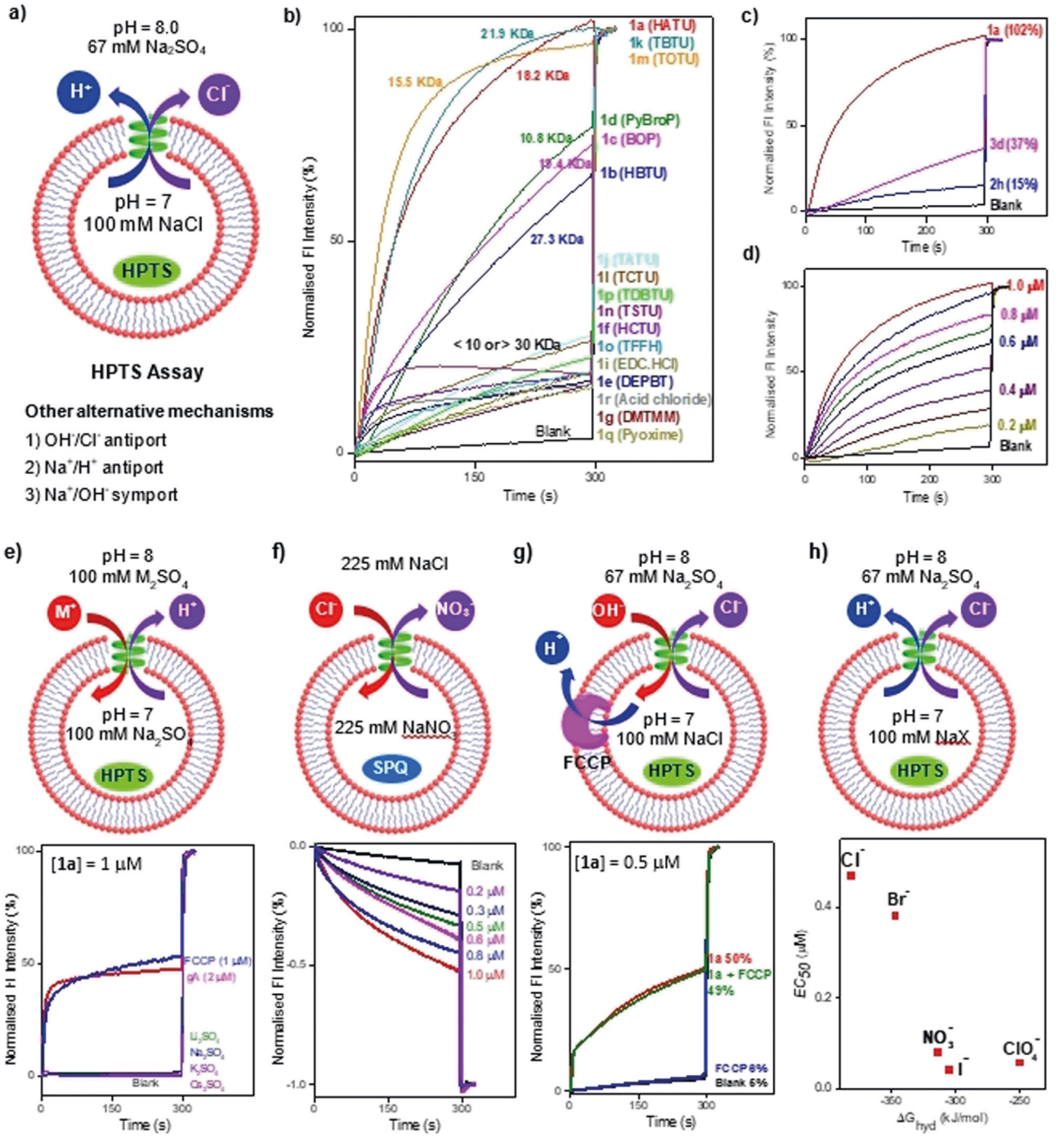

Figure 2. a) Evaluation of ion-transport activity of ion channels through a pH-sensitive HPTS assay and possible mechanisms. b) Ion-transport activities of **1a**–**g** and **1i**–**r** at 1 μM. c) Comparison of ion-transport activities of the best channels **1a**, **2h**, and **3d** from their respective categories **1**, **2**, and **3** at 1 μM. d) Dose-dependent transport activities of **1a**. e) HPTS assay with varied extravesicular cations (M_2SO_4) for studying cation selectivity. f) SPQ assay by nitrate/chloride exchange for confirming chloride as the transport species. g) FCCP-coupled HPTS assay for elucidating the role of proton in chloride transport. h) HPTS assay with varied intravesicular anions (NaX) for studying anion selectivity and determining the corresponding EC_{50} values. In b–e) and g) fluorescence intensity after addition of Triton X-100 at $t = 300$ s was set to 100%.

these are results of poor solubility of **2** and too good a solubility of **3** in buffer at 1 μM. Overall, the polymer channels **1** display much better activities than **2** and **3**, likely because of their more favoured lipophilic character, which leads to more efficient channel incorporation into the lipid membrane. **1a**, the most active channel among 53 polymer channels, was assessed in a dose-dependent manner for Hill Analysis (Figures 2d; see Figure S14). The calculated EC_{50} value of 0.47 μM (0.31 mol% relative to lipid) indicates an excellent ion-transport activity by **1a**.

Preferential transport of anions over cations

For the HPTS assay used to monitor ion-transport activities, incremental changes in fluorescence could be due to ion exchange through antiport (H^+/Na^+ and Cl^-/OH^-) or symport (H^+/Cl^- and Na^+/OH^-) mechanisms. To discern these mechanisms, three sets of assays were performed (Figures 2e–g). At first, both H^+ and Na^+ transports were evaluated using LUVs containing HEPES (10 mM) and Na_2SO_4 (100 mM) at pH 7.0, which were dispersed in the same buffer (10 mM HEPES, 100 mM Na_2SO_4) at pH 8.0. Channel **1a** at 1 μM was found to be nonresponsive towards transport of both H^+ and Na^+. In contrast, both ion transporter gramicidin A (gA) at 2 μM and proton transporter FCCP (carbonyl cyanide 4-(trifluoro methoxy)phenylhydrazone) at 1 μM result in substantial transport activity (Figure 2e). These results rule out both an H^+/Na^+ antiport and Na^+/OH^- symport as the likely mechanisms. Similarly, both variation of extravesicular metal ions ($M^+ = Li^+$, K^+ and Cs^+, Figure 2e), and the assay with very high salt gradients (200 mM Na_2SO_4/K_2SO_4; see Figure S15) reveal very low transport of cations, confirming that it is anions, not cations, that mainly participate in the ion-transport process.

Next, SPQ [6-methoxy-*N*-(3-sulfopropyl)quinolinium] whose fluorescence intensity decreases in the presence of increasing concentrations of Cl^- was introduced into extravesicular region of LUVs (Figure 2f).[18] The observed concentration-dependant quenching of SPQ for channel **1a** at 0.2–1.0 μM provides direct proof of **1a**-mediated chloride influx into LUV.

To additionally differentiate the transport rates between Cl^- and OH^- or H^+, proton transporter FCCP was applied in the HPTS assay (Figure 2g).[18] That transport activities of **1a** (0.5 μM) were found to be comparable in either the presence (49%) or absence (50%) of FCCP suggests H^+ or OH^- transport rates to be faster than that of Cl^-, which constitutes the rate-limiting step. Further, molecular dynamics (MD) results clearly point to the formation of the water chains (see Supporting movie SM3), and these water chains should facilitate rapid transport of H^+, not OH^-, by the Grotthuss mechanism across membranes to maintain the charge balance.

Membrane integrity in the presence of polymer channels

Membrane integrity in the presence of channel molecules was then established by a carboxyfluorescein-leakage assay ($\lambda_{ex} = 492$ nm, $\lambda_{em} = 517$ nm; see Figure S16). Specifically, addition of **1a** at 1 μM causes only a 4% increase in carboxyfluorescein fluorescence, while Melittin, which induces membrane lysis, results in 56% and 91% increases at 0.15 and 0.2 μM, respectively. These comparative data demonstrate that **1a** does not lysate the membrane and possesses a pore size of less than 1 nm across.

To exclude other possible membrane defects (spaces between bundles of polymer tubes, interface between the gel and fluid phases of lipids surrounding the polymer tubes, etc.) that may be responsible for the observed anion transport, **1a** was modified at its two ends using a sterically bulky benzyl group ($W \times L = 6.7 \times 8.3$ Å) to generate the polymer **1a-Bn** (see Scheme S2). Modification of **1a** with a monobenzyl group should not exert significant changes in its helical conformation since the strong intramolecular hydrogen bonds will only direct these benzyl groups to point toward the channel's interior, rather than exterior. Thus, it is expected that **1a-Bn** differs insignificantly from **1a** in terms of association with the membrane lipids, and any possible membrane defects formed by **1a** should also persist for **1a-Bn**. Differing from **1a**, the inward-pointing benzyl groups in **1a-Bn** should at least partially block the channel cavity of 6.5 Å, resulting in either a reduction or complete loss in anion-transport activity. Experimentally, **1a-Bn** indeed becomes incapable of transporting any anions (see Figure S17), thereby supporting the notion that anion transport was mediated by the pore contained in **1a**, rather than membrane defects.

Chloride transport by a channel mechanism and Cl^-/K^+ selectivity

The ability of **1a** to transport anions by a channel mechanism was unambiguously confirmed by the observed single channel current traces for chloride transport, recorded in a planar lipid bilayer at various voltages in symmetric baths (*cis* chamber = *trans* chamber = 1M KCl, Figure 3a). Linear fitting of a current–voltage (*I–V*) plot gives rise to a Cl^- conductance value (γ_{Cl}) of 1.19 ± 0.024 pS for **1a** (Figure 3a), with a Cl^-/K^+ selectivity of 13 (Figures 3b; see Figure S18).

High selectivity and high efficiency in iodide transport

Using the HPTS assay illustrated in Figure 2h, selectivity in **1a**-mediated anion transport was investigated by replacing intravesicular NaCl with NaX ($X^- = Br^-$, I^-, NO_3^-, and ClO_4^-). From the determined EC_{50} values obtained after correcting background signals (Figure 2h; see Figure S19), a selectivity topology, $I^- > ClO_4^- > NO_3^- > Br^- > Cl^- > SO_4^{2-}$, was obtained with I^- ($EC_{50} = 0.042$ μM, or 0.028 mol% relative to lipid) being transported 8 and 10 times faster than Br^- ($EC_{50} = 0.38$ μM) and Cl^- ($EC_{50} = 0.47$ μM), respectively. And both ClO_4^- ($EC_{50} = 0.057$ μM) and NO_3^- ($EC_{50} = 0.08$ μM) are also preferred transport species for **1a**. From these EC_{50} values, the transport selectivity of I^-/K^+ is estimated to be greater than 145. Significantly, in LUVs containing 33% cholesterol, known to decrease membrane fluidity prominently, **1a** still functions well, with EC_{50} values of 0.37 and 0.45 μM for I^- and ClO_4^-, respectively (see Figures S20 and S21).

To compare with Kim's highly selective iodide channel based on a porphyrin-derived covalent organic cage,[8b] the same assay conditions used by Kim were applied to **1a** (see Figure S22). The resulting quenching of HPTS fluorescence follows the same selectivity sequence as reported. Remarkably, **1a**-mediated iodide influx results in 100% quenching at $[\mathbf{1a}] = 0.15$ μM, with mere 14% and 8% for Br^- and Cl^-,

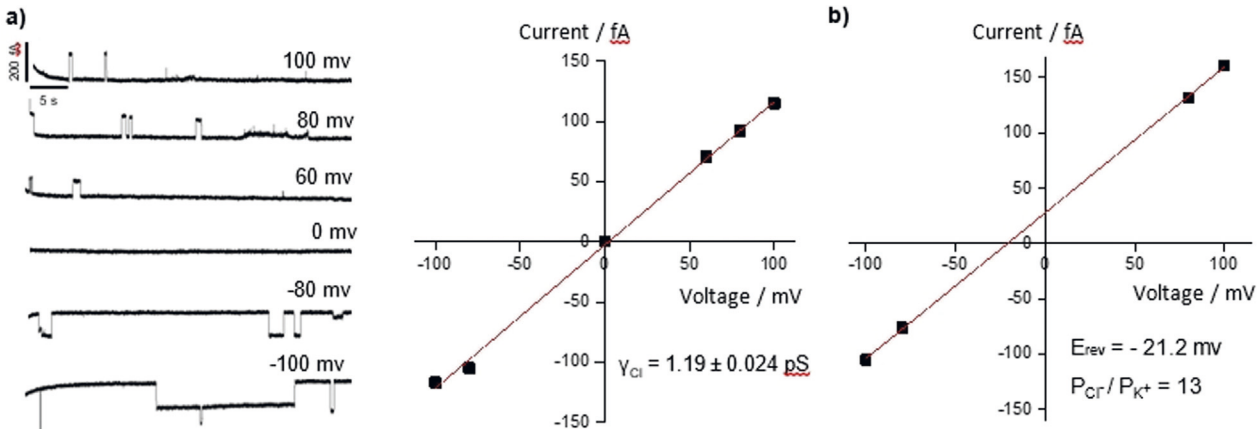

Figure 3. a) Single-channel current traces recorded at various voltages recorded in symmetric baths (*cis* chamber = *trans* chamber = 1 M KCl; linear fitting of current–voltage (I–V) plot gives Cl^- conductance value (γ_{Cl}) of 1.19 ± 0.024 pS for **1a**-mediated transport of chloride. b) Linear fitting of current–voltage (*I–V*) plot gives Cl^-/K^+ selectivity of 13 for **1a**-mediated transport of chloride. For the corresponding current traces, see Figure S18.

respectively. On the basis of initial rate constants (see Figure S22), I^-/Cl^- selectivity was determined to be 42. Compared to **1a**, Kim's organic cage is more selective by 30% ($I^-/Cl^- = 60$), but its iodide transport activity is at least 17 times less active (EC_{50} value > 0.5 mol%).

Lastly, to eliminate possible quenching effects the heavy iodine atom might have on the fluorescence intensity of the HPTS day, we have carried out titration experiments in the presence of iodide anions at concentrations ranging from 10 to 140 mM at pH values 7 and 8 (see Figure S23). We found that at either pH 7 or 8, a change in iodide concentration from 10 to 140 mM produces no more than 2% difference in fluorescence intensity of the HPTS dye when compared to that at 100 mM. These data confirm that anions such as iodides exert insignificant influence on the HPTS dye. In contrast, changes in pH from 7 to 7.5 or from 7 to 8 result in dramatic increases by 96% and 195%, respectively, in fluorescence intensity of the HPTS dye, demonstrating that HPTS dye is indeed far more sensitive to changes in pH than those in iodide concentration, and that our observed iodide transport is not a result of fluorescence quenching by iodide anions.

Computational insights into preferential transport of anions over cations

To elucidate the microscopic mechanism of ion permeation through the polymeric channels, we built an all-atom model of the **HP24** channel containing 24 **A** and 24 **B** units and a height of 2.8 nm using the structure building tool psfgen plugin of VMD[19] (see Figure S8a and Supporting Movies SM1 and SM2). The model was embedded in a patch of 1-palmitoyl-2-oleoyl-sn-glycero-3-phosphatidyl choline (POPC) membrane, which has a hydrophobic thickness of 2.8 nm. To characterize the structural dynamics and ion selectivity of **HP24**, we created several systems by solvating the membrane-embedded **HP24** channel with aqueous solutions of KCl, KI, NaCl, and NaI at either 0.6 or 1 M. Figure S8b shows a typical configuration of a fully assembled all-atom simulation system.

First, we performed equilibrium MD simulations of the systems using a previously described simulation protocol.[20,21] Briefly, the channel was initially restrained, allowing lipid molecules to equilibrate around the channel. After 100 ns, the channel was released, and the system was simulated free of any restraints for 550 ns. During this unrestrained equilibration, the channel maintained its initial structure, with local structural fluctuations stabilizing at about 3.5 Å root mean squared deviation value (see Figure S8c). As soon as the simulation began, water molecules were observed to permeate through the interior cavity of the channel, from one side of the membrane to the other. Within the 550 ns equilibrium of the 0.6 M NaCl system, we observed five Cl^- ions entering and passing the channel, without observing Na^+ transport.

We computationally assessed the ability of the **HP24** channel to conduct ions by simulating the channel solvated in a 1M solution of KCl, KI, NaCl, or NaI under ±1 V transmembrane voltage. Figure 4a shows a typical simulation system. Figure 4b plots the total charge transported through the channel as a function of simulation time for the KCl and KI systems, and Figure S9 shows similar data for the NaCl and NaI systems. The slope of the charge versus time trace yields the average currents for all simulated systems (see Table S3). In all the cases studied, the current was predominately carried by anions (Cl^- and I^-), which contributed from 78 to 93% of the total current (Figure 4c; see Figure S9). While these simulations undoubtedly demonstrate the ability of **HP24** to conduct ions in an anion-selective manner, direct comparison of the simulated currents with experiment is not possible.[22] Further, the channel was observed to conduct more current under the negative transmembrane bias than under the positive bias. This rectification of ionic current can be explained by the presence of the negatively (COO^-) and positively (NH_3^+) charged group at the either entrance of the channel (Figure 4a).

To determine the near-equilibrium energetics of ion transport through the **HP24** channel and its dependence on

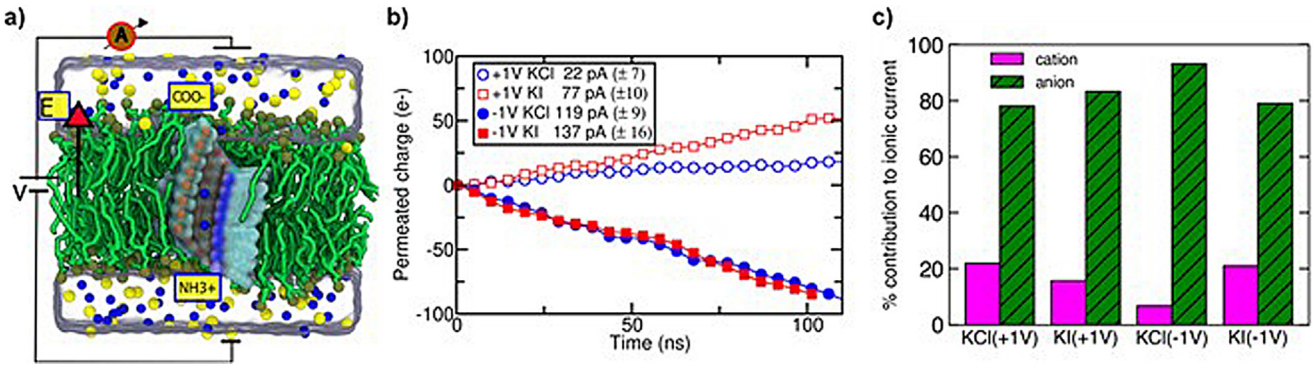

Figure 4. Ionic-current through the **HP24** channel simulated using the all-atom MD method. a) A cut-away view of the simulation system where the channel is shown as a molecular surface with colors according to the local atom types: red (oxygen), blue (nitrogen), and cyan (carbon). The yellow labels specify the location of the terminal groups of the channels. Nitrogen atoms of the lipid head groups are shown as tan sphere whereas the tails of the lipid molecules are shown as thick green lines. K^+ (yellow) and Cl^- (blue) ions (at 1 M concentration) are shown as spheres whereas the volume occupied by water is represented by a semi-transparent surface. b) The total permeated charge (integrated ionic current) as a function of the simulation time in the units of the elementary charge, e. The slope of each line gives the average current. The inset specified the average current values with the error bars for each system. c) Percentage of total current carried by the cation and anion species in the simulations of the KCl and KI systems.

ion species, we performed replica exchange umbrella sampling MD simulations.[23] The simulation system was divided into 69 windows using 1 Å bins arranged along the Z axis (the axis normal to the lipid bilayer plane). An ion was confined to remain within the respective windows using a harmonic potential (Figure 5a). The starting configuration for each window was obtained from a brief (1.4 ns) steered molecular dynamics (SMD) run. All 69 simulations were run in parallel for abut 100 ns using the replica exchange umbrella sampling protocol.[24] Figure 5b shows the resulting potential of mean force (PMF) of Cl^-, K^+, and I^- ions with respect to its Z coordinate. K^+ ion PMF is characterized by a single barrier in the middle of the membrane. The PMFs of Cl^- and I^- ions are qualitatively different: after initial increase, the PMF is largely flat in the middle of the channel, with some variations among the plateau that we attribute to local deformation of the channel's structures, in particular small fenestration at $Z = 10$ Å. With regard to the barrier amplitude, K^+ experiences the largest energy penalty, with the I^- ions being smallest Thus, consistent with our experimental results, the PMF profiles clearly support both anion selectivity relative to cation and I^- selectivity with respect to the Cl^- ion. The presence of the periodic fine structure in the PMF of the I^- ion ($-15 < Z < 0$) suggests a pronounced effect of the channel's chemical structure on the energetics of I^- conductance. Figure S10a shows similar data for NaCl system, that is, the Cl^- ions are transported preferentially over Na^+ ions.

To determine the molecular mechanism of the ion selectivity, we examined hydration of ions in bulk solutions and when passing through the channel. First, we defined the solvation shell of each ion type from the water-ion radial distribution functions[25] (see Figure S11). Figure 5c plots the average number of water molecules in the first solvation shell of the respective ion with respect to the ion's Z coordinate. Owing to its largest ionic radius, the I^- ion possesses the largest solvation shell in the bulk followed by the Cl^- and K^+ ions The solvation shell of the I^- ions, however, loses the greatest number of water molecules as it enters in the channel. In fact, there are fewer water molecules surrounding the I^- ion in the channel than those surrounding the Cl^- ion. This result, however, does not explain anion selectivity of the channel. By analyzing equilibrium MD trajectories,[26] we obtained the electrostatic potential map of the system (Figure 5d). The average electrostatic potential inside the central lumen of the channel is positive as compared to the bulk solution (Figure 5e), making the channel selective for anion transport. Finally, it has been suggested that the rate of transport through a channel is conditioned by the number of hydrogen bonds that the solute makes with the channel.[27] To see if this applies also to transport of solvated ions, we computed the average number of hydrogen bonds formed between the water molecules in the first solvation shell of the ion and the remaining part of the system (e.g., channel's interior functional groups as well as other water molecules not from the first solvation shell, Figure 5f). We found that the solvation shell of I^- forms a fewer number of hydrogen bonds as compared to Cl^-, thereby giving rise to a more frictionless, faster transport of the I^-.

Overall, the analysis of the simulations trajectories confirms that the channel is highly selective for anions, with the energetic barriers being lower for anions than those for cations. These reduced energy penalties in anion transport arise from a positive electrostatic potential of the central lumen rendered by the many methyl groups (from methoxy groups) that decorate the lumen. Corroborated by ionic current measurements in the applied electric field simulations and with the smallest energy barrier for I^- relative to others (e.g., Na^+, K^+, nd Cl^-), as seen from the free-energy calculations using an enhanced sampling method, it is evident that the **HP24** channel is most favorable for the transport of I^-. And a fewer number of the hydrogen bonds formed by the water molecules in the first solvation shell of I^- provides the molecular basis that accounts for its faster more frictionless transmembrane transport than for Cl^-.

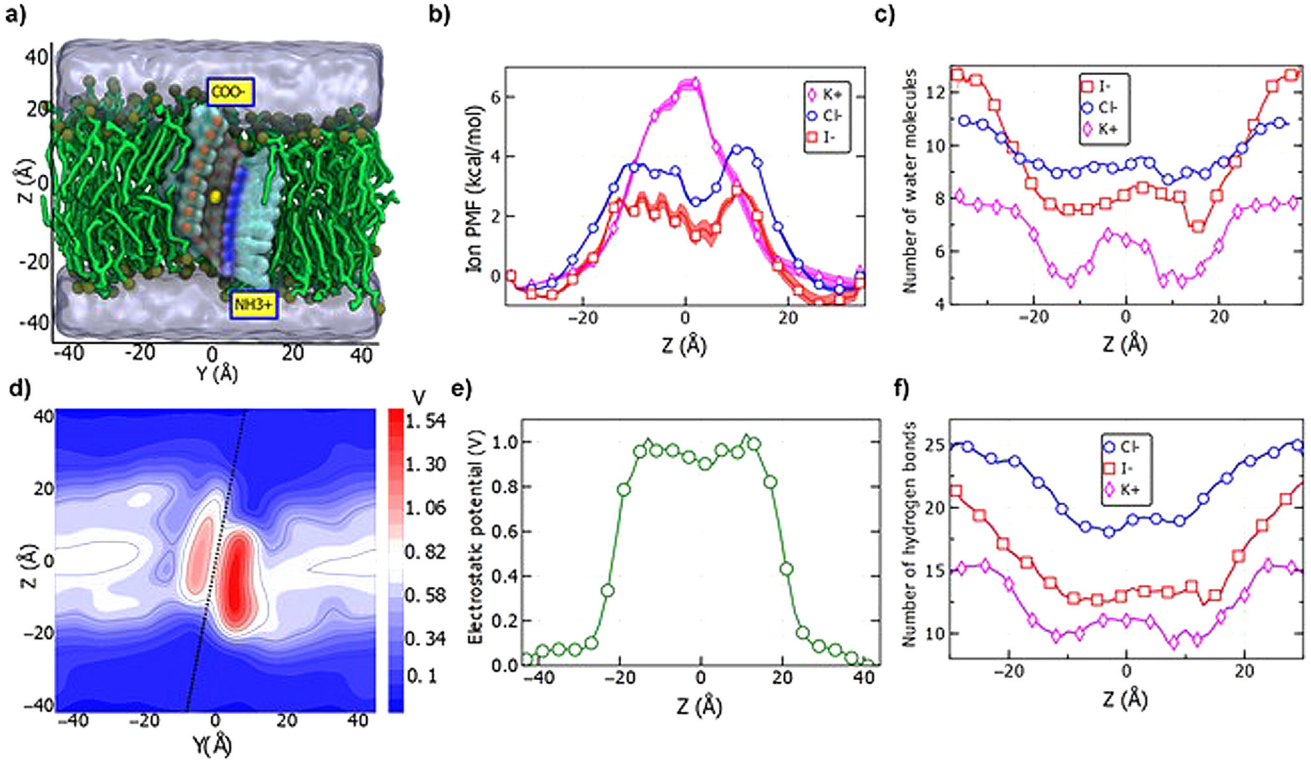

Figure 5. Free-energy and molecular mechanism of ion permeation through an **HP24** channel. a) Cut-away view of the simulation system used for replica-exchange umbrella sampling simulation. In each replica system, a single ion was harmonically restrained to the center of a 1 Å wide window; 69 such windows spanned the full range of Z-values in 1 Å interval. b) The free energy of ions permeating across the membrane through the **HP24** channel. The shadowed region shows the standard error in the measurements of PMF. c) The average number of water molecules in the first solvation shell of the permeating ion as a function of its position along the bilayer normal (*z*-axis). d) An electrostatic potential map of the **HP24** channel in lipid bilayer membrane averaged over 50 ns of equilibrium MD simulation using the PMEpot plugin of VMD. A dotted blue line passing through the center shows the tilted axis of the channel along the bilayer normal. e) The average electrostatic profile along the transmembrane pore of the channel (dotted line in Figure 5 d). The potential values were averaged over a 2 Å cylinder coaxial with the axis of the channel. f) The average number of hydrogen bonds formed by the water molecules from the ion's first solvation shell with the rest of the system versus the *Z* coordinate of the ion.

Conclusion

In summary, we have for the first time achieved efficient one-pot preparation of fully hydrogen-bonded helically folded aromatic foldamer-based nanotubes of 6.5 Å across and up to 14 nm in helical height, by using simple amide coupling agents such as HATU. These nanotubes carry an extensive array of oxygen atoms along their interior surface but are found to preferentially transport anions rather than cations. Moreover, lipophilicity and proper length were found to be crucial, with the most active polymer channel **1a** carrying shorter octyl side chains and having a helical height of 3.6 nm. This polymer-based channel 1) displays an intrinsic excellent selectivity towards anions over cations, 2) prefers iodide over other inorganic anions with iodide being transported more than 10 times better than chloride, and 3) functions well in a cholesterol-rich environment. Anion selectivity was confirmed and the origin of such selectivity was elucidated by all atom MD simulation studies. Given a high modularity in repeating units, a broad variety of polyhydrazide-based nanotubes, which possess a hollow cavity of wide-ranging diameters, can be readily envisioned for interesting applications.

Acknowledgements

This work was supported by the Institute of Bioengineering and Nanotechnology (Biomedical Research Council, Agency for Science, Technology and Research, Singapore), the Singapore National Research Foundation under its Environment and Water Research Programme and administered by PUB, the National Science Foundation (USA) under grant DMR-1827346, and the National Institutes of Health under grant P41-GM104601. Supercomputer time was provided through the Early Allocation grant on Frontera (FTA-Chemla), XSEDE Allocation Grant no. MCA05S028 and the Blue Waters petascale supercomputer system at the University of Illinois at Urbana-Champaign.

Conflict of interest

The authors declare no conflict of interest.

Keywords: hydrogen bonds · ion channels · iodide · molecular dynamics · supramolecular chemistry

How to cite: *Angew. Chem. Int. Ed.* **2020**, *59*, 4806 – 4813
Angew. Chem. **2020**, *132*, 4836 – 4843

[1] C. Duran, C. H. Thompson, Q. Xiao, H. C. Hartzell, *Annu. Rev. Physiol.* **2010**, *72*, 95 – 121.
[2] a) F. Ahad, S. A. Ganie, *Indian J. Endocrinol. Metab.* **2010**, *14*, 13 – 17; b) H. R. Chung, *Ann. Pediatr. Endocrinol. Metab.* **2014**, *19*, 8 – 12.
[3] E. Darrouzet, S. Lindenthal, D. Marcellin, J.-L. Pellequer, T. Pourcher, *Biochim. Biophys. Acta Biomembr.* **2014**, *1838*, 244 – 253.
[4] A. Mina, E. J. Favaloro, J. Koutts, *Lab. Med.* **2011**, *42*, 744 – 746.
[5] a) V. Sidorov, F. W. Kotch, G. Abdrakhmanova, R. Mizani, J. C. Fettinger, J. T. Davis, *J. Am. Chem. Soc.* **2002**, *124*, 2267 – 2278; b) P. H. Schlesinger, R. Ferdani, J. Liu, J. Pajewska, R. Pajewski, M. Saito, H. Shabany, G. W. Gokel, *J. Am. Chem. Soc.* **2002**, *124*, 1848 – 1849; c) V. Gorteau, G. Bollot, J. Mareda, A. Perez-Velasco, S. Matile, *J. Am. Chem. Soc.* **2006**, *128*, 14788 – 14789; d) V. Gorteau, G. Bollot, J. Mareda, S. Matile, *Org. Biomol. Chem.* **2007**, *5*, 3000 – 3012; e) X. Li, B. Shen, X.-Q. Yao, D. Yang, *J. Am. Chem. Soc.* **2009**, *131*, 13676 – 13680; f) C. R. Yamnitz, S. Negin, I. A. Carasel, R. K. Winter, G. W. Gokel, *Chem. Commun.* **2010**, *46*, 2838 – 2840; g) A. Vargas Jentzsch, S. Matile, *J. Am. Chem. Soc.* **2013**, *135*, 5302 – 5303; h) T. Saha, S. Dasari, D. Tewari, A. Prathap, K. M. Sureshan, A. K. Bera, A. Mukherjee, P. Talukdar, *J. Am. Chem. Soc.* **2014**, *136*, 14128 – 14135; i) T. Saha, A. Gautam, A. Mukherjee, M. Lahiri, P. Talukdar, *J. Am. Chem. Soc.* **2016**, *138*, 16443 – 16451; j) X. Wei, G. Zhang, Y. Shen, Y. Zhong, R. Liu, N. Yang, F. Y. Almkhaizim, M. A. Kline, L. He, M. Li, Z.-L. Lu, Z. Shao, B. Gong, *J. Am. Chem. Soc.* **2016**, *138*, 2749 – 2754; k) S. V. Shinde, P. Talukdar, *Angew. Chem. Int. Ed.* **2017**, *56*, 4238 – 4242; *Angew. Chem.* **2017**, *129*, 4302 – 4306; l) H. Behera, N. Madhavan, *J. Am. Chem. Soc.* **2017**, *139*, 12919 – 12922; m) C. Ren, X. Ding, A. Roy, J. Shen, S. Zhou, F. Chen, S. F. Yau Li, H. Ren, Y. Y. Yang, H. Q. Zeng, *Chem. Sci.* **2018**, *9*, 4044 – 4051.
[6] a) J. T. Davis, O. Okunola, R. Quesada, *Chem. Soc. Rev.* **2010**, *39*, 3843 – 3862; b) P. R. Brotherhood, A. P. Davis, *Chem. Soc. Rev.* **2010**, *39*, 3633 – 3647; c) S. Matile, A. Vargas Jentzsch, J. Montenegro, A. Fin, *Chem. Soc. Rev.* **2011**, *40*, 2453 – 2474; d) D. S. Kim, J. L. Sessler, *Chem. Soc. Rev.* **2015**, *44*, 532 – 546.
[7] a) X. Wu, L. W. Judd, E. N. W. Howe, A. M. Withecombe, V. Soto-Cerrato, H. Li, N. Busschaert, H. Valkenier, R. Pérez-Tomás, D. N. Sheppard, Y.-B. Jiang, A. P. Davis, P. A. Gale, *Chem* **2016**, *1*, 127 – 146; b) S.-K. Ko, S. K. Kim, A. Share, V. M. Lynch, J. Park, W. Namkung, W. Van Rossom, N. Busschaert, P. A. Gale, J. L. Sessler, I. Shin, *Nat. Chem.* **2014**, *6*, 885; c) B. A. Smith, M. M. Daschbach, S. T. Gammon, S. Xiao, S. E. Chapman, C. Hudson, M. Suckow, D. Piwnica-Worms, G. W. Gokel, W. M. Leevy, *Chem. Commun.* **2011**, *47*, 7977 – 7979.
[8] a) N. Madhavan, E. C. Robert, M. S. Gin, *Angew. Chem. Int. Ed.* **2005**, *44*, 7584 – 7587; *Angew. Chem.* **2005**, *117*, 7756 – 7759; b) B. P. Benke, P. Aich, Y. Kim, K. L. Kim, M. R. Rohman, S. Hong, I.-C. Hwang, E. H. Lee, J. H. Roh, K. Kim, *J. Am. Chem. Soc.* **2017**, *139*, 7432 – 7435.
[9] J.-L. Hou, X.-B. Shao, G.-J. Chen, Y.-X. Zhou, X.-K. Jiang, Z.-T. Li, *J. Am. Chem. Soc.* **2004**, *126*, 12386 – 12394.
[10] P. Xin, P. Zhu, P. Su, J.-L. Hou, Z.-T. Li, *J. Am. Chem. Soc.* **2014**, *136*, 13078 – 13081.
[11] a) D.-W. Zhang, H. Wang, Z.-T. Li, *Macromol. Rapid Commun.* **2017**, *38*, 1700179; b) J.-Y. Chen, J.-L. Hou, *Org. Chem. Front.* **2018**, *5*, 1728 – 1736; c) F. Chen, J. Shen, N. Li, A. Roy, R. J. Ye, C. L. Ren, H. Q. Zeng, *Angew. Chem. Int. Ed.* **2020**, *59*, 1440 – 1444; *Angew. Chem.* **2020**, *132*, 1456 – 1460.
[12] D.-W. Zhang, X. Zhao, J.-L. Hou, Z.-T. Li, *Chem. Rev.* **2012**, *112*, 5271 – 5316.
[13] a) Y. Hamuro, S. J. Geib, A. D. Hamilton, *Angew. Chem. Int. Ed. Engl.* **1994**, *33*, 446; *Angew. Chem.* **1994**, *106*, 465; b) J. Zhu, R. D. Parra, H. Q. Zeng, E. Skrzypczak-Jankun, X. C. Zeng, B. Gong, *J. Am. Chem. Soc.* **2000**, *122*, 4219 – 4220; c) V. Berl, I. Huc, R. G. Khoury, M. J. Krische, J. M. Lehn, *Nature* **2000**, *407*, 720 – 723.
[14] J. J. van Gorp, J. A. J. M. Vekemans, E. W. Meijer, *Chem. Commun.* **2004**, 60 – 61.
[15] a) BOP = ((Benzotriazol-1-yloxy)tris(dimethylamino)phosphoniumhexa fluorophosphate); b) Z. Y. Du, C. L. Ren, R. J. Ye, J. Shen, Y. J. Lu, J. Wang, H. Q. Zeng, *Chem. Commun.* **2011**, *47*, 12488 – 12490.
[16] H. Q. Zeng, R. S. Miller, R. A. Flowers, B. Gong, *J. Am. Chem. Soc.* **2000**, *122*, 2635 – 2644.
[17] C. Ren, J. Shen, H. Q. Zeng, *J. Am. Chem. Soc.* **2017**, *139*, 12338 – 12341.
[18] C. L. Ren, F. Zeng, J. Shen, F. Chen, A. Roy, S. Zhou, H. Ren, H. Q. Zeng, *J. Am. Chem. Soc.* **2018**, *140*, 8817 – 8826.
[19] W. Humphrey, A. Dalke, K. Schulten, *J. Mol. Graph.* **1996**, *14*, 33 – 38.
[20] K. Göpfrich, C.-Y. Li, I. Mames, S. P. Bhamidimarri, M. Ricci, J. Yoo, A. Mames, A. Ohmann, M. Winterhalter, E. Stulz, A. Aksimentiev, U. F. Keyser, *Nano Lett.* **2016**, *16*, 4665 – 4669.
[21] K. Decker, M. Page, A. Boyd, I. MacAllister, M. Ginsberg, A. Aksimentiev, *ACS Biomater. Sci. Eng.* **2017**, *3*, 342 – 348.
[22] There are several reasons that could explain the difference between simulated and measured currents. 1) The applied potential is typically concentrated to the transmembrane region, with limited effect on ion entrance. That is, the high bias might wash out some barriers in the middle of the channel, without affecting the barriers at the channel entrance. This scenario may explain why rectification is more pronounced at 1 V. 2) With regard to rectification, it is also possible that the terminal groups in the experiment do not maintain the same conformation as in simulations. Such partial unwinding is more likely on the experimental time scale. Without the charged group present right at the entrance of the channel, the rectification phenomenon should not happen. 3) There are potential inaccuracies regarding the channel structure and parameterization.
[23] Y. Sugita, A. Kitao, Y. Okamoto, *J. Chem. Phys.* **2000**, *113*, 6042 – 6051.
[24] B. Roux, *Comput. Phys. Commun.* **1995**, *91*, 275 – 282.
[25] C. N. Rowley, B. t. Roux, *J. Chem. Theory Comput.* **2012**, *8*, 3526 – 3535.
[26] A. Aksimentiev, K. Schulten, *Biophys. J.* **2005**, *88*, 3745 – 3761.
[27] A. Horner, F. Zocher, J. Preiner, N. Ollinger, C. Siligan, S. A. Akimov, P. Pohl, *Sci. Adv.* **2015**, *1*, e1400083.

Manuscript received: December 19, 2019
Accepted manuscript online: January 16, 2020
Version of record online: February 4, 2020

